




Evaluation of electrochemical performance of antimony modified screen-printed carbon electrodes

Alexander B. Kifle ^{a*} , Nataliya Malakhova ^a , Alexandra Ivoilova ^a ,
Nataliya Leonova ^b , Svetlana Saraeva ^a, Alisa Kozitsina ^a 

a: Department of Analytical Chemistry, Institute of Chemical Technology, Ural Federal University, Ekaterinburg 620002, Russia

b: Department of Technology of electrochemical devices and materials, Institute of Chemical Technology, Ural Federal University, Ekaterinburg 620002, Russia

* Corresponding author: tsionaomi@gmail.com



This paper belongs to a Regular Issue.

Abstract

This study compares the electrochemical performance of screen-printed carbon electrodes (SPCEs) modified with antimony (Sb/SPCEs) under different potentiostatic pre-plating conditions. Neutral Red (NR) was employed as a novel redox probe to evaluate the electrochemical performance of Sb/SPCEs. It was demonstrated that NR in the protonated form performs quasi-reversible redox transformations at bare SPCE and Sb/SPCEs in phosphate buffer solutions (pH 5.5±0.5) in the potential range of (−0.30)–(−0.75) V, where the antimony is not electroactive. Sb/SPCEs were studied electrochemically by cyclic voltammetry (CV) / electrochemical impedance spectroscopy (EIS), and morphologically by scanning electron microscopy (SEM). Cyclic voltammetry investigations revealed the dependence of the electrochemical performance of Sb/SPCEs on the degree of coverage of the substrate with the metal. The obtained CV, EIS, and SEM data are consistent. The lowest charge transfer resistance (R_{ct}) value (6 Ω) was obtained at Sb/SPCE with the highest degree of antimony coverage. To investigate the electroanalytical performance of Sb/SPCEs, nickel (II) ions were utilized as a model analyte. A study of roughness factors and sensitivity towards nickel (II) ions for Sb/SPCEs using two-tailed Pearson's criterion revealed a high degree of correlation between their electrochemical and electroanalytical properties. The results show that using NR as a redox probe can help controlling modification processes during the development of innovative antimony-containing sensors.

Keywords

screen-printed carbon electrodes
antimony film
neutral red
electrochemical/
morphological characteristics
stripping voltammetry

Received: 07.03.24

Revised: 25.03.24

Accepted: 28.03.24

Available online: 09.04.24

Key findings

- Neutral red was used as redox probe for comparative evaluation of the electrochemical performance of SPCEs modified with antimony.
- CV experiments showed an increase in the electroactive surface area of Sb/SPCEs compared to the bare-SPCE, depending on surface morphology.
- The obtained SEM, cyclic voltammetry and EIS data are in good agreement.
- A good correlation between electrochemical and electroanalytical characteristics of Sb/SPCEs was observed.
- NR as a redox probe can help controlling modification processes during the development of innovative antimony-containing sensors.

© 2024, the Authors. This article is published in open access under the terms and conditions of the Creative Commons Attribution (CC BY) license (<http://creativecommons/licenses/by/4.0/>).

1. Introduction

For many years, mercury-based electrodes, i.e., hanging mercury drop electrodes and mercury film electrodes, have been extensively used as the ideal working electrodes for

electrochemical determination of heavy metal ions and some electroactive organic compounds [1–3]. This is mainly attributed to their remarkable features, such as high reproducibility, renewability, sensitivity, wide cathodic potential window, and ability to form amalgams with many metals.

Nevertheless, the potential toxicity of mercury and its salts led to the search for alternative environmentally-friendly “green” electrodes [4].

Electrode materials, including carbon, gold, and platinum, have been applied as substitutes for mercury, but none of them exhibits electroanalytical performance comparable to that of mercury [5, 6]. However, over the last two decades, less toxic bismuth, antimony, and tin sensors have been introduced [7–11].

Bismuth-based electrodes show desirable electrochemical characteristics similar to those of mercury electrodes. Moreover, bismuth electrodes are less toxic and insensitive to dissolved oxygen, which makes them more preferable substitutes for mercury and other solid electrodes [12–14]. As a result, they have been widely utilized in various electroanalytical applications [11]. Following bismuth film electrodes (BiFEs), in 2007, antimony film electrodes (SbFEs) were reported by Hocevar et al. as another functional and environmentally acceptable electrode material [15]. Compared to BiFEs, SbFEs exhibit comparable electroanalytical performance with extra advantages such as a relatively wide operational potential window associated with favorably hydrogen evolution and an unexpectedly low re-oxidation signal for the antimony itself [15–19]. Among other features, the antimony electrode revealed better performance in more acidic conditions ($\text{pH} \leq 2$). Lately, tin-film electrodes (SnFEs) were proposed as sensors for trace metal analysis [20]. It was reported that SnFEs are environmentally less toxic and show satisfactory analytical characteristics; hence, they can serve as environment-friendly electrodes.

The development of these environment-friendly modified electrodes involves a variety of supporting materials, mostly carbon-based, such as glassy carbon, boron-doped diamond, carbon paste, carbon fiber and screen-printed electrodes [21]. Recently, screen-printed carbon electrodes (SPCEs) have been introduced as the best alternative substrates [22–24]. The screen-printing technology allows the mass production of highly reproducible, disposable, single-use SPCEs at a reduced cost with different electrode geometries and provides great versatility of modification procedures applications [11].

In-situ prepared antimony based electrodes are mostly used in the analysis of Pb(II) and Cd(II) with anodic stripping voltammetry [15, 25–28]. Ex-situ preplated SbFEs are reported, as a rule, for the determination of metal ions that do not form alloys with the electrode material during the preconcentration step and organic substances [5, 18, 29–33]. Cathodic voltammetry, including adsorptive stripping voltammetry, is used for such cases. Unlike SbFEs, SnFEs are used in less frequent applications only via in-situ approaches and are devoted to anodic stripping voltammetry (ASV) of trace metals [20, 34, 35].

The kinetic and thermodynamic features of many chemical processes, as well as the electrical characteristics of materials and the electrode-electrolyte interfaces, can be

quantitatively evaluated using cyclic voltammetry (CV) and electrochemical impedance spectroscopy (EIS) techniques [36]. Typically, these techniques make use of near-reversible redox couples such as $[\text{Fe}(\text{CN})_6]^{3-}/[\text{Fe}(\text{CN})_6]^{4-}$ or $[\text{Ru}(\text{NH}_3)_6]^{3+}/[\text{Ru}(\text{NH}_3)_6]^{2+}$ [37, 38]. The redox potentials of these probes in solutions with a pH of 5–6, which are working ones for “classic” redox couples, extend to the anodic potential region where antimony films undergo dissolution from substrate surface [39]. The exceptions are electrodes with trace amounts of antimony on the surface, precipitated in-situ from solutions with a low concentration of antimony ions (1–2 mg/L) [15, 25, 28]. As for SnFEs, there is no problem with “classic” redox couples because the metal does not dissolve in solutions with a pH of 5–6 [20].

In our previous work, we proposed to use the monoprotonated 3-Amino-7-dimethylamino-2-methylphenazine hydrochloride (Neutral Red, NR) as an alternative to “classic” redox couples for comparative quantitative evaluation of the electrochemical characteristics of screen-printed carbon electrodes modified with bismuth under various metal deposition conditions [40]. A good correlation was established between the morphological, electrochemical, and electroanalytical characteristics of these electrodes.

This work aims to apply the developed approach for quantitative evaluation of the electrochemical characteristics of screen-printed carbon electrodes ex-situ modified with antimony under various metal deposition conditions. Additionally, it seeks to determine the possible correlations between the morphological, electrochemical, and electroanalytical characteristics of Sb/SPCEs using nickel (II) ions as a model analyte.

2. Experimental

2.1. Reagents and apparatus

All chemicals used in this work were of analytical grade and were used as received without further purification. Acids, salts, alkalis, and absolute ethanol (95 wt.%) were received from Russian manufacturers (Prime Chemicals Group, Labtech, JSC Medkhimprom, Uralkali and Lenreactive, Russia). Neutral Red (≥ 90 wt.%) and potassium ferricyanide/potassium ferrocyanide ($[\text{Fe}(\text{CN})_6]^{3-}/[\text{Fe}(\text{CN})_6]^{4-}$) were supplied by Sigma-Aldrich (USA). Dimethylglyoxime (DMG, 99 wt.%) was purchased from Merck (Germany). Phosphate buffer solutions (PBS) (0.05 M, pH 5) were prepared by mixing suitable phosphate solutions of Na_2HPO_4 and KH_2PO_4 in appropriate volumetric ratios. Ammonia buffer solution (pH 9.8 ± 0.2) was made by mixing ammonia solution and ammonium chloride. A 0.1 M stock solution of NR was prepared by dissolving an appropriate amount of NR in water. A 0.025 M DMG solution was prepared in 95% ethanol. Stock solutions of Ni(II) and of Sb(III) ions with a mass concentration of 1 g/L were purchased from “Prime Chemicals Group” (Moscow region, Mytishchi, RF). Deionized water obtained on device DVS-M/1HA(18)-N (“Mediana filter,” Russia) was used throughout this study.

PC-controlled 884 Professional VA and μ Autolab Type III potentiostat/galvanostat (Metrohm, Switzerland) equipped with a magnetic stirrer and standard three-electrode cells were used for electrochemical research and EIS measurements. Sinusoidal voltage disturbance with an amplitude of 10 mV was applied in the frequency range 0.1–10⁶ Hz at pre-selected potentials of the model system according to the data of Neutral Red cyclic voltammograms. Fitting to electrical equivalent circuits was performed with NOVA 1.11 software.

SPCEs based on carbon-containing paste DuPont 7102 from DuPont (USA) ex-situ modified with antimony served as the working electrodes. An Ag/AgCl (3 M KCl) as a reference electrode and a glassy carbon rod as an auxiliary electrode were used in the measurements. SPCEs were laboratory-made using a screen-printing machine (TIC-50B, China). The carbon-containing ink layer, about 40 μ m thick, was applied through a mesh stencil onto a textolite polymer substrate strips (0.2x3.8 cm) of 0.035 cm thickness (ZAO "Elektroizolit", Russia). The strips were heat-treated in a drying cabinet per the regulations of the ink manufacturer and insulated. The geometric surface area of the working electrodes was about 0.10 cm². The morphology of potentiostatically prepared antimony films was analyzed with a scanning electron microscope (SEM) Tescan Vega with EDX Oxford Xplore 30 (Tescan, Czech Republic) energy dispersive microanalysis system. The average antimony particles size and the surface area of the SPCE covered with antimony (%) were estimated using the program Image Processing and Analysis in Java (<https://imagej.nih.gov/ij/download.html>). A digital "Expert pH ionomer" (Econiks Expert, Russia) was used for measuring the pH of solutions.

2.2. Preparation of Sb/SPCEs

Antimony-modified screen-printed carbon electrodes (Sb/SPCEs) were prepared ex-situ under potentiostatic conditions with solution stirring according to known procedures used for cathodic voltammetry, including adsorptive

stripping voltammetry [18, 29, 30]. After the plating procedure, each Sb/SPCE was rinsed with a 0.01 M HCl solution and immersed in the test solution.

2.3. Voltammetric procedure

Linear calibration plots were obtained for the determination of Ni(II) on an ex-situ Sb/SPCEs, with increasing metal concentration in 0.2 M NaCl + 0.02 M ammonia buffer (pH 9.5 \pm 0.5) + 0.25 mM dimethylglyoxime [5, 16, 30]. Adsorptive preconcentration of the Ni(II)-DMG complex on the Sb/SPCEs was carried out at -0.75 V with accumulation time of 30 s in stirred solution. After the accumulation and the equilibration period of 10 s, a differential pulse voltammetric scan (initial potential, -0.75 V; final potential, -1.20 V; pulse amplitude, 0.05 V; pulse step, 0.006 V; scan rate, 0.06 V/s) was applied to the working electrode, and the voltammogram was recorded. Then, the electrode was cleaned from traces of remaining adsorbed complex for 10 s at -1.30 V under stirring.

3. Results and discussion

3.1. Morphological characterization of Sb/SPCEs

Conditions for the ex-situ electrodeposition of antimony on different substrates are presented in Table 1. This approach is often used owing to the simplicity of the preparation protocol and the electroanalytical performance of the electrodes prepared by this method [9, 11, 42].

Systematic studies on the influence of plating conditions on the surface morphology of SbFEs in contrast to BiFEs have not been conducted. From the available plating conditions (Table 1), we chose plating conditions that were proposed for the determination of Ni(II) [18, 30] and Pb(II), Cd(II) [29] ions by cathodic adsorptive stripping voltammetry using dimethylglyoxime [18, 30] and pyrogallol red [29] as complexing agents. These conditions were chosen to obtain Sb/SPCE-1 [18], Sb/SPCE-2 [29], and Sb/SPCE-3 [30] with significantly different morphologies.

Table 1 Conditions for potentiostatic pre-plating of the antimony films on the substrate surface used in the method of cathodic adsorptive stripping voltammetry.

Substrate	Analyte	Antimony plating solution	Deposition conditions		Ref.
			E_{el} (V) ^b	t_{el} (s) ^c	
GCE ^a	Ni(II)	0.01 M HCl + 10 mg/L Sb(III)	-0.5	60	[5]
SPCE	Ni(II)	0.01 M HCl + 50 mg/L Sb(III)	-0.5	300	[18]
GCE/Nafion	Pb(II), Cd(II)	0.5 M HCl + 100 mg/L Sb(III)	-1.2	50	[29]
GCE	Ni(II)	0.01 M HCl + 10 mg/L Sb(III)	-1.0	120	[30]
SPCE	Pd(II)	0.01 M HCl + 50 mg/L Sb(III)	-0.5	300	[31]
GCE	Pantoprazole	0.01 M HCl + 20 mg/L Sb(III)	-0.7	60	[41]
GCE	4,6-dinitro-o-cresol	acetic buffer (pH 4.5) + 6 mg/L Sb(III)	-1.0	60	[33]
GCE	Sulfasalazine	0.01 M HCl + 20 mg/L Sb(III)	-0.7	60	[43]

^a GCE – Glassy carbon electrode;

^b E_{el} – electrodeposition potential;

^c t_{el} – electrodeposition time.

As per reference [28], the Sb film on the ex-situ prepared Sb/SPCE surface was formed by randomly dispersed and firmly fixed Sb particles ranging in size from 0.5 to 2 μm , which, most notably, did not completely cover the underlying carbon surface. With the electroplating conditions used in [30], microscopic examination of the surface of electroplated SbFEs by SEM revealed a low coverage of their surface with antimony, characterized by scarce and widely dispersed antimony particles.

SEM was used to investigate the morphology of the Sb/SPCEs surfaces. SEM images for Sb/SPCEs surface (Figure 1) show the effect of the different plating conditions on the morphology of the films.

SEM image of bare-SPCE (Figure 1a) displays a rough electrode surface predominantly composed of inhomogeneous carbon substrate. Dispersed bright tinges are shown at the edges of the graphite particles, possibly due to more secondary electrons emitted from them. Antimony film on Sb/SPCE-1 surface (Figure 1b) is characterized mainly by the formation of more or less evenly distributed tiny Sb particles with an average size of $0.6 \pm 0.1 \mu\text{m}$. Most of the Sb nucleation is favored at the elevated sites of a rough electrode surface, most probably due to the relatively high electric field at the elevated sites in comparison to that on the smooth area. In addition to this, a few randomly distributed, irregularly shaped large dendrite Sb particles with an average size of $4 \pm 1 \mu\text{m}$ are observed. The total surface covered by Sb is calculated to be 12%.

The micrograph for Sb/SPCE-2 (Figure 1c) shows the formation of widely dispersed fine Sb grains with an average particle size of $1.0 \pm 0.3 \mu\text{m}$ in diameter, with the electrode surface clearly exposed. These Sb particles cover ca. 4% of the substrate surface. As for Sb/SPCE-3 (Figure 1d), due to the small amount of Sb in the plating solution, very small particles are formed that are invisible in the SEM images, even with the highest possible resolution for the microscope we used.

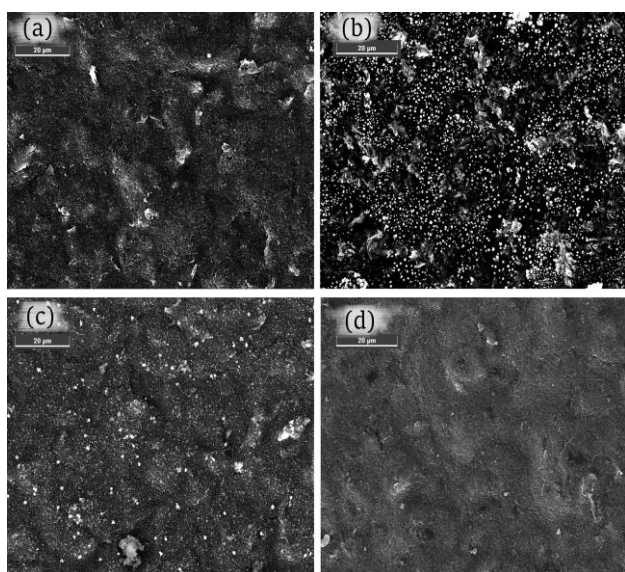


Figure 1 SEM images of SPCE surfaces before and after modification: bare-SPCE (a), Sb/SPCE-1 (b), Sb/SPCE-2 (c), Sb/SPCE-3 (d).

Despite this, ImageJ software analysis estimates the surface coverage by Sb particles to be around 1%. These results indicate the dependence of antimony morphology on the chosen plating conditions (Sb concentration, pH of the plating solution, deposition potential, and deposition time).

3.2. Electrochemical behavior of NR at bare-SPCE and Sb/SPCEs

pH-dependent reduction of monoprotonated NR (NRH^+) ($\text{pK}_a = 6.81$ [44]) in an aqueous medium at a glassy carbon electrode occurs in two steps, each requiring a single electron transfer. The first step: (NRH^+) \leftrightarrow radical (NRH^\bullet) is a reversible process [45]. As per [45], the electrochemical changes of monoprotonated NR in an aqueous medium are depicted in Figure 2.

As can be seen from Figure 3c, NR behaves in a similar way at Sb/SPCE-1 in 0.05 M PBS + 0.1 M NaNO_3 . This solution is typically used as a supporting electrolyte in the study of NR redox transformations [46]. Two single-electron peaks of NR reduction are recorded at -0.53 V and -0.82 V .

CV registered from -1.2 V to 1.2 V at Sb/SPCE-1 in 0.05 M PBS + 0.1 M NaNO_3 solution (Figure 3b) exhibited a large and broad anodic peak with a $435 \mu\text{A}$ maximum, corresponding to the dissolution of deposited antimony film, in the potential range of -0.4 V to 1.2 V . As shown in Figure 3a, the characteristic potential range of $[\text{Fe}(\text{CN})_6]^{3-/4-}$ activity lies in the potential range where it is completely masked by antimony oxidation current from the Sb/SPCE-1 surface. So, this redox probe is inconvenient for characterizing antimony modified SPCEs. On the other hand, NR in the protonated form undergoes redox transformations in the potential range of (-0.3) – $(-0.9) \text{ V}$, in which antimony is not electroactive (Figure 3c).

For bare-SPCE, the value of the potential difference between the peaks for the oxidation / reduction currents (ΔE) of the $[\text{Fe}(\text{CN})_6]^{3-/4-}$ pair is 1.02 V (Figure 3a). On the other hand, the NR redox process exhibits a peak separation of 0.07 V (Figure 3c), approximately one and a half orders of magnitude less, due to the strong electron transfer ability of NR as a redox mediator [47].

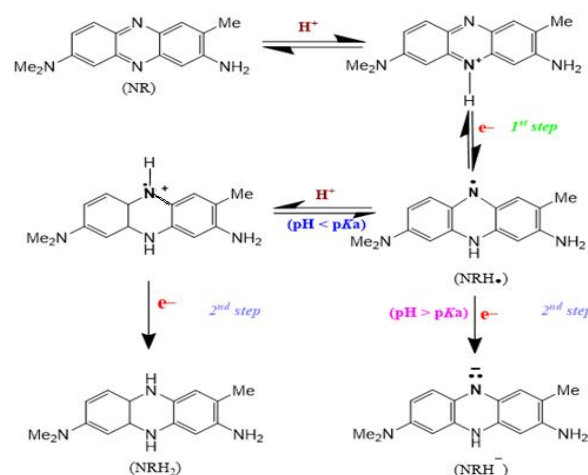


Figure 2 Schematic mechanism of NR redox changes depending on pH.

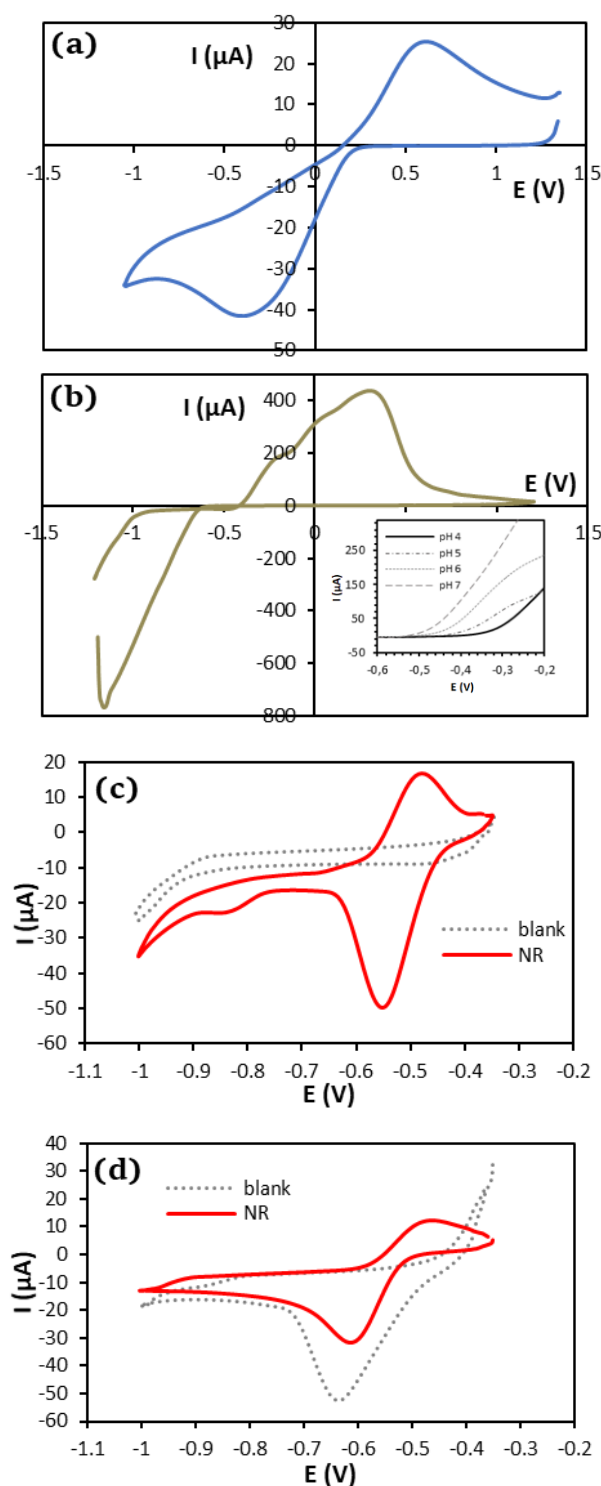


Figure 3 CVs registered in 0.05 M PBS + 0.1 M NaNO₃ with a scan rate of 0.1 V/s at: bare-SPCE after addition of 5 mM [Fe(CN)₆]^{3-/4-} (a); Sb/SPCE-1 (b); Sb/SPCE-1 without and with addition of 0.5 mM NR (c, d). Buffer solution pH 5.0 (a-c) and 7.0 (d).

The effect of solution pH on the dissolution of antimony film from Sb/SPCE-1 in the potential range of -0.6 to -0.2 V is shown in Figure 3b (inset). As can be seen, a rise in the pH of the electrolyte solution resulted in a shift of the potential for antimony dissolution toward more negative values. The produced Sb(III) ions are easily hydrolyzed at higher pHs [14], which facilitates the oxidation process and leads to a shift of the anodic potential to a more negative

range with increasing pH [13]. Therefore, we can observe the reduction current of antimony ions from the near-electrode layer in neutral PBS in the absence of NR (Figure 3d, blank). As a result, the optimal pH value in this study was chosen as 5.0 ± 0.5 .

3.3. The dependence of NR response on scan rate

The influence of the potential scan rate on the cathodic currents of 0.05 mM NR on bare and antimony-modified SPCEs was investigated using CV over a range of scan rates of 0.01–0.60 V/s, as given in Figure 4(a, b). It was observed that the peak heights of NR increase, and the peak potential shift to a more negative value with increasing scan rates. The peak current is correlated linearly with the square root of the potential scan rate, as follows: for bare-SPCE: $I_p (\mu A) = 15.44 \cdot v^{1/2} (V/s)^{1/2} - 0.24 \mu A$, $R^2 = 0.998$; (Figure 4c, red curve); for Sb/SPCE-1: $I_p (\mu A) = 45.47 \cdot v^{1/2} (V/s)^{1/2} - 3.09 \mu A$, $R^2 = 0.987$ (Figure 4c, blue curve).

A linear relationship between the logarithm of peak current vs. logarithm of scan rate with a slope value of 0.51, $R^2 = 0.997$ was obtained for bare-SPCE (Figure 4d, red curve). These results suggest that the electrochemical process at bare-SPCE, as for the glassy carbon electrode [45], is diffusion-controlled. Nevertheless, for Sb/SPCE-1, a straight line with a slope value of 0.64, $R^2 = 0.995$ (Figure 4d, blue curve) was acquired, indicating a diffusion process accompanied by adsorption [48].

3.4. Electrochemical characterization and electrochemical impedance spectroscopy study

Cyclic voltammetry and EIS, with NR as a redox probe, were used to study the electrochemical characteristics of bare-SPCE and Sb/SPCEs. Cyclic voltammograms and Nyquist plots obtained for these electrodes are shown in Figures 5a and 5c, respectively. Every Nyquist curve was recorded at a working potential, which was chosen based on the corresponding CV voltammogram.

As the electrochemical process at bare and antimony-modified SPCEs is mainly controlled by diffusion, the electroactive surface areas (A) of the investigated electrodes were calculated based on the CV data (Figure 5a) using the Randles-Ševčík equation (1) for reversible systems:

$$I_p = (\pm 2.69 \cdot 10^5) n^{3/2} A D^{1/2} C v^{1/2}, \quad (1)$$

where A is the electroactive area (cm^2), I_p is the the anodic or cathodic peak current, D is the the diffusion coefficient of the electroactive species in solution ($2.28 \cdot 10^{-6} \text{ cm}^2/\text{s}$ for NR) [49], C is the concentration of the redox system in the background electrolyte ($5 \cdot 10^{-8} \text{ mol}/\text{cm}^3$), and n is the number of electrons involved in the redox process ($n = 1$). To calculate A , slopes of the I_p vs $v^{1/2}$ plots (Figure 4c) were used. The data obtained from CVs are presented in Table 2.

The modification of SPCEs with antimony increased the electroactive surface area of Sb/SPCEs by a factor of 3.0 and 1.8 compared to the bare-SPCE for Sb/SPCE-1 and Sb/SPCE-2, respectively.

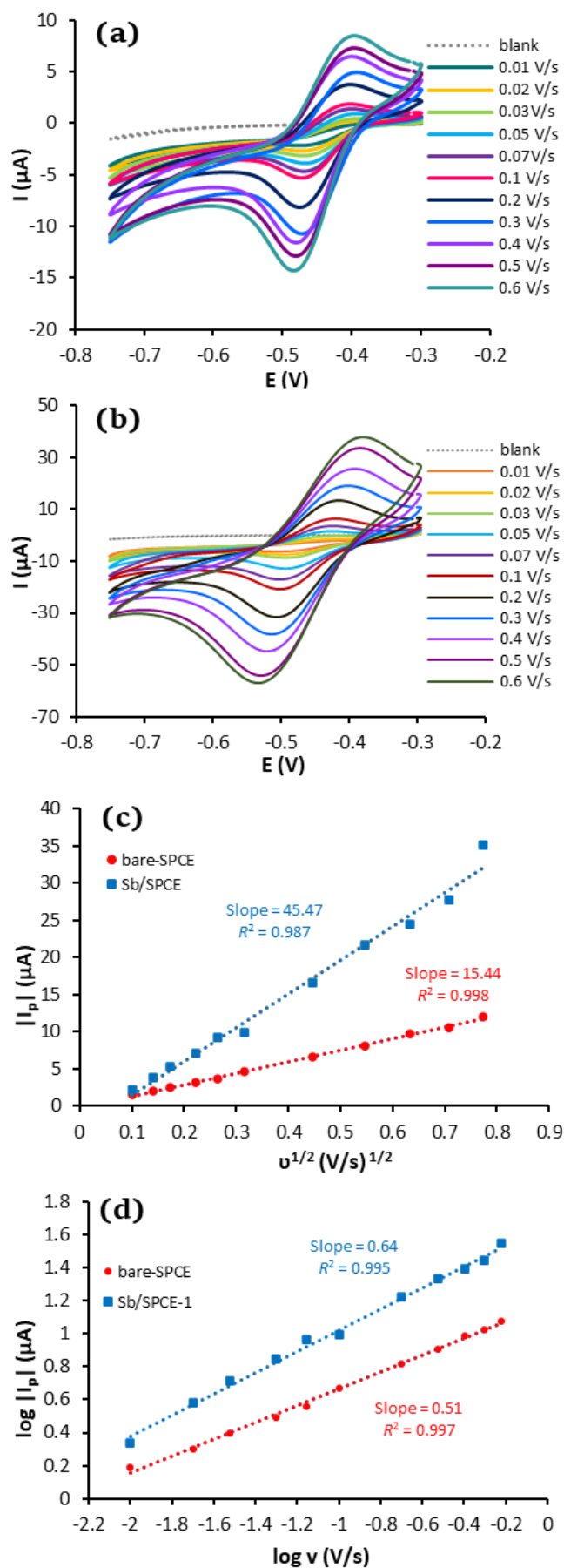


Figure 4 CVs voltammograms of NR registered at: bare-SPCE (a) and Sb/SPCE-1 in 0.05 M PBS + 0.1 M NaNO₃ + 0.05 mM NR (pH 5.0) at a scanning rate of 0.01 - 0.6 V/s (b). Analysis of corresponding peak currents as a function of scan rate (c, d).

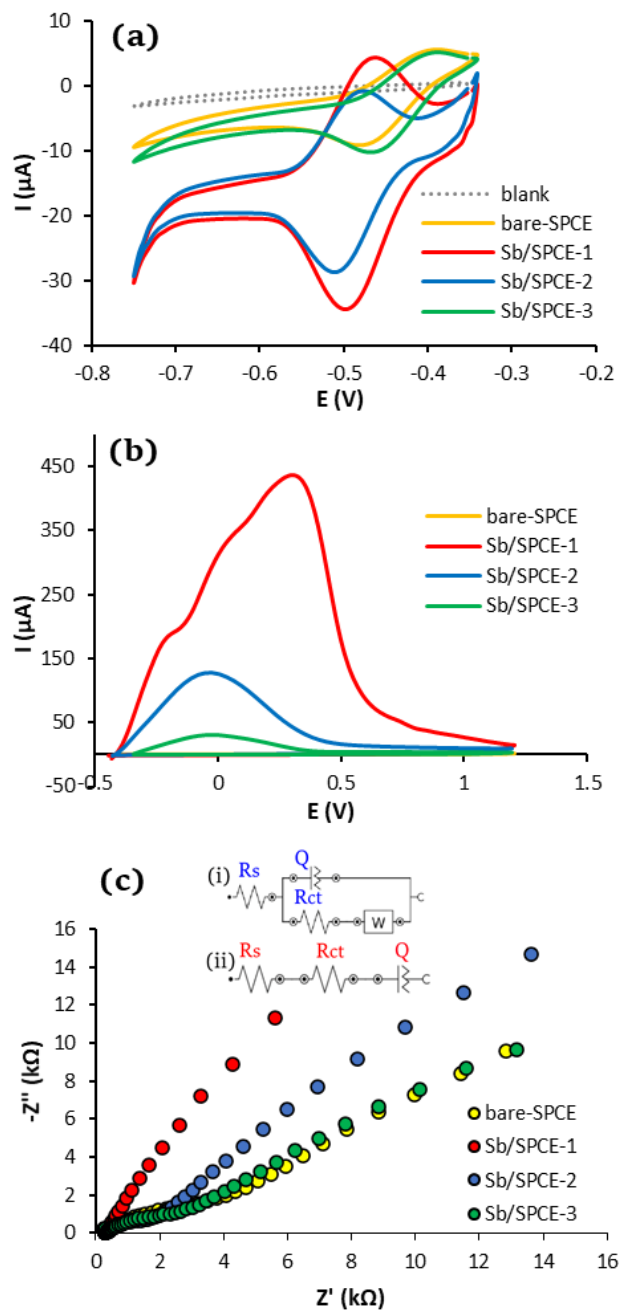


Figure 5 Cyclic voltammograms (a and b), Nyquist curves recorded in 0.05 M phosphate buffer solution + 0.1 M NaNO₃ (pH 5.0) (c) without (b) and with addition of 0.05 mM Neutral Red on bare-SPCE and Sb/SPCEs (a and c). Randles equivalent electrical circuits for bare-SPCE and Sb/SPCE-2, Sb/SPCE-3 (c, i). Modernized model of an ideally polarizable electrode with a distributed double-layer capacitance for Sb/SPCE-1 (c, ii). Scan rate = 0.30 (a) and 0.1 V/s (b).

Sb/SPCE-1 exhibited the highest *A* value in comparison to the other electrodes, as expected from the SEM image of antimony film (Figure 1b). As for Sb/SPCE-3, in this regard there is little difference between it and bare-SPCE because the surface of the substrate is almost entirely exposed.

Figure 5b compares the cyclic voltammetry curves of antimony dissolution registered from -0.4 V to 1.2 V at Sb/SPCEs in 0.05 M PBS + 0.1 M NaNO₃ solution at a scan rate of 0.1 V/s. Sb/SPCE-1 shows a higher integrated area.

The specific areal capacitance (*C_s*) values for Sb/SPCEs were calculated from the CV curves using Equation (2) [52]:

$$C_s = \frac{\int I(V)dV}{A_g v \Delta V} \quad (2)$$

where I is the oxidation current, $\int I(V)dV$ is the integrated area of the CV curve, A_g is the electrode's geometric area (cm^2), v is scan rate (V/s), and ΔV is the potential window (V).

As can be seen from Table 2, C_s is values for Sb/SPCEs correlate well with their electroactive / specific electroactive surface area. This is due to the dependence of both C_s and A on the amount of metal on the substrate surface. The obtained result is in agreement with the conclusions of several studies where it was shown that the increase in electrochemical capacity result in enhanced specific surface area [50, 51]. Quite good convergence of the results of assessing the electroactive area of Sb/SPCEs using Randles-Ševčík equation with independent method confirms the effectiveness of NR in the evaluation of electrochemical performance of antimony modified electrodes.

For all electrodes (Table 2), the value of the potential difference between the peaks for the oxidation/reduction current (ΔE) does not exceed 0.08 V, and reduction/oxidation peak currents ratio (I_{pc}/I_{pa}) is closed to 2.5. This indicates a quasi-reversible behavior of NR at the interface of bare and antimony modified SPCEs. As for Sb/SPCEs-1, 2 $I_{pc}/I_{pa} = 1.6$ and peak separation of 0.04–0.05 V for a one-electron transfer point to the near-reversible nature of the processes.

Detailed analysis of the data (presented in the Table 2) obtained during an electrochemical impedance measurement was performed by fitting the experimental data with an equivalent circuit, based on the Boukamp model with NOVA 1.11 software and based on literary data [52, 53]. The obtained value of χ^2 does not exceed 0.1 (Table 2).

According to research [40], the most probable model for describing surface phenomena in the metal – NR system is the generalized Randles equivalent electrical circuit (EEC) (Figure 5c(i)). It describes a mixed kinetic- and diffusion-

controlled process that corresponds to the diffusion process, accompanied by adsorption, in the system under study (Sb/SPCEs – NR). EEC consists of the uncompensated resistance (R_Ω) with a parallel combination of the charge transfer resistance (R_{ct}), a constant phase element (Q), and diffusion, which is represented by the Warburg diffusion element (W). The majority of the R_Ω is due to the solution resistance (R_s). The R_{ct} represents the difficulty of electron transfer of the NR redox probe between the solution and the electrode, thus giving information on the electrode surface. Q models non-ideal capacitance. The diffusion resembles the mass transfer of the species from or to the electrode's surface during the EIS measurements. The results of impedance spectra processing with generalized Randles EEC for bare-SPCE, Sb/SPCE-2 and Sb/SPCE-3 are presented in Table 2.

To describe the Nyquist diagrams obtained on Sb/SPCE-1, we used a modified circuit of an ideally polarizable electrode with a distributed double-layer capacitance (Figure 5c(ii)) [52]. In the system under study, there is also an uncompensated resistance (R_Ω) with a series combination of charge transfer resistance (R_{ct}). Due to the heterogeneity of the electroactive surface of the electrode, considering also the diffusion part of the double electrical layer, the simplest way to model these changes relative to an ideally polarized electrode is to represent C_{dl} as a constant-phase element (Q) of the capacitive type. Thus, as in the case of the generalized Randles equivalent electrical circuit, the element Q models a non-ideal capacitor.

According to the SEM data (Figure 1b), Sb/SPCE-1 surface differs significantly from other electrodes in that the largest substrate surface area is coated with metallic antimony in the form of fairly evenly distributed, finely dispersed antimony particles. This is probably why the electroactive surface area, C_s and Q values for this film are the highest (Table 2). The calculated exponential factor for Sb/SPCE-1 $N=0.8$ (Table 2) corresponds to the values given in Stoynov et al. [52].

Table 2 Electrochemical characterization of electrodes studied in 0.05 M phosphate buffer solution + 0.1 M NaNO_3 + 0.05 mM neutral red (pH 5.0).

Electrode	I_{pc}^a (μA)	I_{pa}^b (μA)	I_{pc}/I_{pa}	ΔE^c (V)	A^d (cm^2)	C_s^e (mF/cm^2)	R_s^f (Ω)	R_{ct}^g (Ω)	W^h (μS)	Q^i (μS)	N^j	χ^2^k	Sb_{cov}^l (%)
bare-SPCE	-7.9	3.1	2.5	0.08	0.74	0.1	285	4380	85.9	5.68	0.6	0.081	-
Sb/SPCE-1	-18.7	12.1	1.6	0.04	2.24	17.8	289	6	-	126	0.8	0.069	12
Sb/SPCE-2	-13.1	8.0	1.6	0.05	1.35	4.3	261	1160	75.0	16.6	0.7	0.095	4
Sb/SPCE-3	-8.3	3.5	2.4	0.07	0.81	1.1	309	2780	81.8	11.3	0.6	0.064	1

^a I_{pc} – cathodic peak current;

^b I_{pa} – anodic peak current;

^c ΔE – potential peak separation;

^d A – electroactive area;

^e C_s – specific areal capacitance;

^f R_s – solution resistance;

^g R_{ct} – charge transfer resistance;

^h W – Warburg diffusion element;

ⁱ Q – constant phase element;

^j N – non-uniformity factor;

^k χ^2 – defines one of the convergences criteria;

^l Sb_{cov} – degree of substrate coverage by antimony.

The highest R_{ct} values were obtained at bare-SPCE and Sb/SPCE-3 with a low degree (1%) of substrate coverage by antimony (Sb_{cov}), as shown in Table 2. The lowest R_{ct} value (6 Ω) was measured at Sb/SPCE-1 with the highest degree (12%) of Sb_{cov} . It can be explained by the very good electrical conductivity of metallic antimony. The data obtained are consistent with the well-known fact that EIS can provide information about surface coverage with metal films [54].

3.5. Electroanalytical performance of the Sb/SPCEs towards Ni(II)

Ni(II) ions were used as model analytes to determine the electroanalytical performance of the SPCEs modified with antimony under different deposition conditions (Table 1). The protocols for Ni(II) ion determination by cathodic adsorptive stripping voltammetry using dimethylglyoxime as a complexing agent at antimony-modified electrodes are described in [5, 18, 30].

Characteristics of Ni(II) calibration curves for every type of Sb/SPCEs and corresponding differential pulse (DP) voltammograms of Ni(II) are shown in Figure 6. As can be seen from Figure 6a, for Sb/SPCE-1 the area of reduction current for Ni(II)-dimethylglyoximate (the response) linearly depends on its concentration in the solution in the range of 5–50 $\mu\text{g/L}$. The correlation coefficient is closer to the value of 1 (0.998). In this case, the response shape is symmetrical and can be measured with high precision (Figure 6b). Recoveries for 5 $\mu\text{g/L}$ Ni(II) ($n = 3$, $P = 0.95$) on Sb/SPCE-1 are about 100% and amount to $96 \pm 0.4\%$ (RSD = 3.2%). The limit of detection (LOD) calculated from the regression equation $Q (\mu\text{C}) = (0.0161 \pm 0.0002) C - (0.0059 \pm 0.0026)$ ($R^2 = 0.9981$) for the calibration curve (Figure 6a) in the range of 5–25 $\mu\text{g/L}$ Ni(II) as $3\sigma/\text{slope}$ is 0.5 $\mu\text{g/L}$ Ni(II) ions. It is lower than those reported in [18] as 0.9 $\mu\text{g/L}$ for commercial SPCE provided by DropSens (Spain) with ex-situ pre-plating antimony film under identical conditions.

In the case of using Sb/SPCE-2 (Figure 6c), the linearity of the calibration plot narrows up to 10–40 $\mu\text{g/L}$ Ni(II).

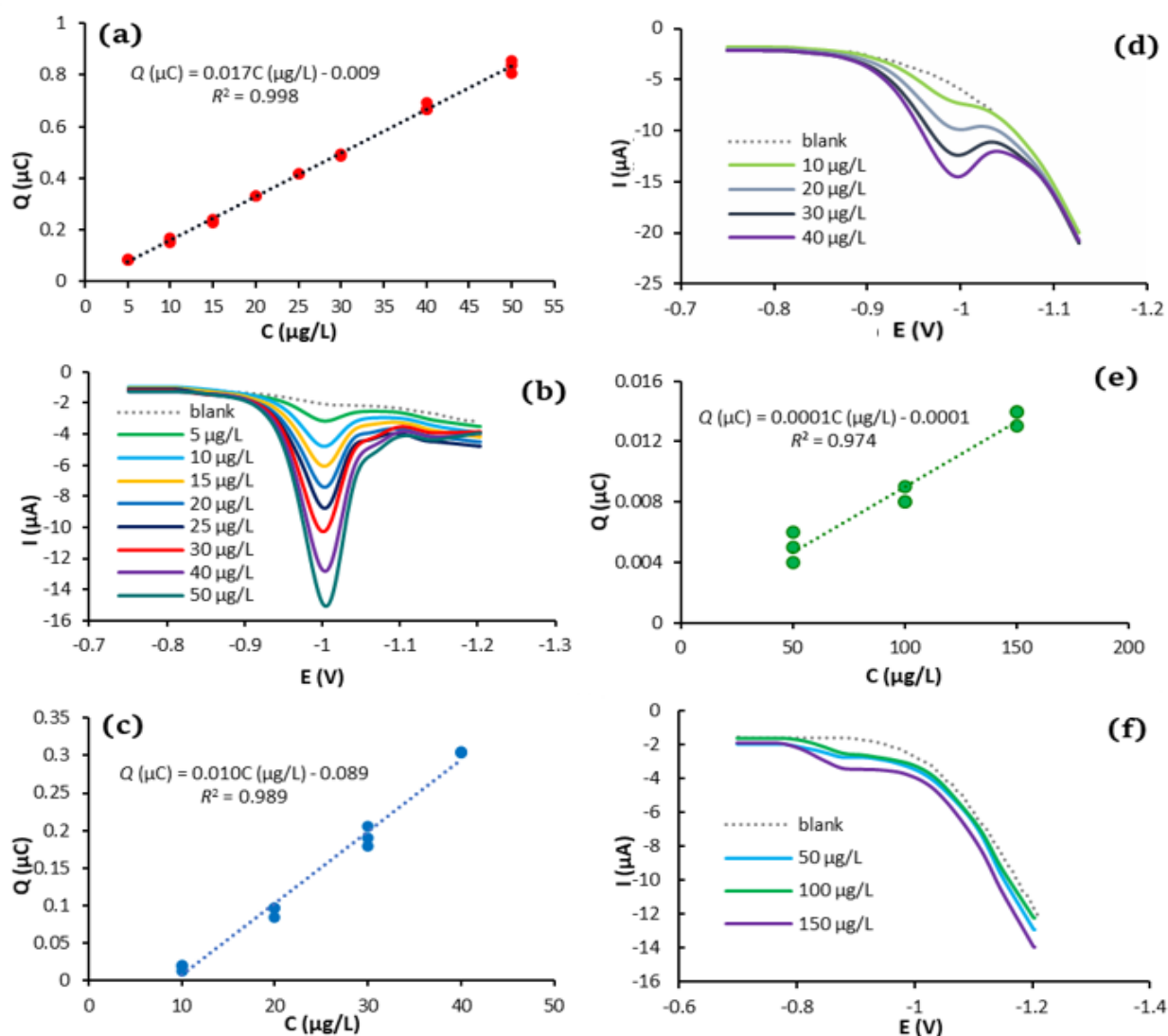


Figure 6 The calibration plots of Ni(II) determination over a concentration range of: 5–50 $\mu\text{g/L}$ at Sb/SPCE-1, with a step of 5 $\mu\text{g/L}$ (a); 10–40 $\mu\text{g/L}$ at Sb/SPCE-2, with a step of 10 $\mu\text{g/L}$ (c) and 50–150 $\mu\text{g/L}$ at Sb/SPCE-3, with a step of 50 $\mu\text{g/L}$ (e). Corresponding DP voltammograms of Ni(II) registered at: Sb/SPCE-1 (b), Sb/SPCE-2 (d) and Sb/SPCE-3 (f) in ammonia buffer (pH 9.5 ± 0.5) + 0.25 mM DMG. DP voltammogram parameters: pulse step 0.006 V, pulse amplitude 0.05 V, scan rate 0.06 V/s. Analysis conditions: $E_{acc} = -0.75$ V, $t_{acc} = 30$ s.

The electrode shows a significant lowering in sensitivity towards Ni(II) ions and asymmetrical shape of the response (Figure 6d), in contrast to the Sb/SPCE-1. The combination of these two factors significantly reduces the possibility of using this electrode for analytical purposes. Recoveries of Sb/SPCE-2 for 10 $\mu\text{g/L}$ Ni(II) ($n = 3$, $P = 0.95$) amount to $7.5 \pm 1.7\%$ (RSD = 9.1%) and indicate a significant systematic underestimation of the analysis results due to the absence of a direct proportional dependence of the response on the concentration of Ni(II) ions in the solution, which makes it inconvenient for analytical purposes.

Sb/SPCE-3 (Figure 6e) shows the lowest sensitivity towards Ni(II) ions, with recoveries for 50 $\mu\text{g/L}$ Ni(II) ($n = 3$, $P = 0.95$) as $110 \pm 33\%$ (RSD = 21%). The correlation coefficient of the calibration plot is reduced significantly (0.943). The slope of the calibration plot for Ni(II) ion determination (Figure 6e) with Sb/SPCE-3 (0.0001 $\mu\text{Q}\cdot\text{L}/\mu\text{g}$) is two orders of magnitude less compared to other Sb/SPCEs (Figures 6a, c). The negligible responses of Ni(II) ions (Figure 6f) are unsuitable for analytical purposes. This may be explained by the very small amount of antimony on the Sb/SPCE-3 surface (Figure 1d) and a low current of dissolving antimony from the Sb/SPCE-3 surface (Figure 5b).

The data for comparing the surface characteristics of Sb/SPCEs with their sensitivity towards Ni(II) are shown in Table 3. The conditions for obtaining experimental data are presented in the corresponding sections.

As we can see, the worst electroanalytical characteristics, including the lowest sensitivity towards Ni(II) ions, are obtained on Sb/SPCE-3 with the least degree of antimony coverage (Figure 1d). The results we obtained for Sb/SPCE-3 are close to the data [30] for GCE with antimony film pre-plating under identical conditions. In this case, no responses from nickel dimethylglyoximate could be registered. According to the authors, the formed structure with low coverage of the GCE surface with antimony possessed low adsorptive properties since adsorption occurs preferentially on the metal (Sb) rather than on the carbon substrate. At the same time, Sb/SPCE-1 is characterized by the greatest sensitivity towards Ni(II) (Table 3). It demonstrates the highest peak current value for NR reduction (Table 2) and, therefore, the highest roughness factors (RF, the ratio of the electroactive surface to the geometrical surface).

Table 3 Comparison of morphological, electrochemical, and electroanalytical characterization of Sb/SPCEs.

Electrode	Particle size (μm)	Sb _{cov} ^a (%)	RF ^b	Sensitivity towards Ni(II) ($\mu\text{C}\cdot\text{L}/\mu\text{g}$)
bare-SPCE	–	–	7.4	–
Sb/SPCE-1	0.6 ± 0.1	12	22.4	0.017
Sb/SPCE-2	1.0 ± 0.2	4	13.5	0.010
Sb/SPCE-3	ND ^c	1	8.1	0.0001

^a Sb_{cov} – degree of substrate coverage by antimony;

^b RF – roughness factor;

^c ND – not detected.

This result can be explained by the formation of the finely dispersed antimony particles (Figure 1b), combined with the largest area of metal coverage of the substrate in comparison with other electrodes (Table 3). On the contrary, Sb/SPCE-3, characterized by a practically bare surface, is distinguished by the lowest RF value.

Comparison of average values of RF and sensitivity to model analyte for Sb/SPCEs with two-tailed Pearson's criterion shows a high degree of correlation between their electrochemical and electroanalytical characteristics with correlation coefficients of 0.994 for Ni(II) ($n = 3$, $R_{\text{crit}} = 0.988$, $P = 0.95$) [55].

4. Conclusions

Neutral red was used as a redox probe for comparative evaluation of the electrochemical performance of screen-printed carbon electrodes (SPCEs) modified with antimony under different deposition conditions (Sb/SPCEs). Cyclic voltammetry experiments showed an increase in the electroactive surface area of Sb/SPCEs compared to the bare-SPCE, depending on surface morphology. The degree of substrate coverage by antimony was assessed with scanning electron microscopy and electrochemical impedance spectroscopy. The obtained SEM, CV, and EIS data are in good agreement. Comparison of RF and Sb/SPCEs sensitivity towards Ni(II) ions as model analytes with Pearson's criterion showed a good correlation between their electrochemical and electroanalytical characteristics. The developed approach might be useful for developing novel antimony-containing sensors as it allows very simple and rapid control of modification processes.

• Supplementary materials

No supplementary materials are available.

• Funding

This work was supported by the Ministry of Science and Higher Education of the Russian Federation (Ural Federal University Program of Development within the Priority-2030 Program).

• Acknowledgments

None.

• Author contributions

Conceptualization: N.M.

Data curation: N.M.

Formal Analysis: A.B.K., A.I., N.L.

Funding acquisition: A.K.

Investigation: A.B.K., A.I., N.L., S.S.

Methodology: A.B.K., A.I., N.L.

Project administration: A.K.

Resources: A.K.

Software: A.K.

Supervision: A.K.

Validation: N.M., A.K.

Visualization: A.B.K., A.I., N.L., S.S.

Writing – original draft: A.B.K., A.I.

Writing – review & editing: N.M.

● Conflict of interest

The authors declare no conflict of interest.

● Additional information

Author IDs:

Alexander B. Kifle, Scopus ID [57875710700](#);

Nataliya Malakhova, Scopus ID [6701723934](#);

Alexandra Ivoilova, Scopus ID [57211981729](#);

Nataliya Leonova, Scopus ID [57352201500](#);

Svetlana Saraeva, Scopus ID [26647714200](#);

Alisa Kozitsina, Scopus ID [16432620500](#).

Website:

Ural Federal University, <https://urfu.ru/en/>.

References

- Toghill KE, Wildgoose GG, Moshar A, Mulcahy C, Compton RG. Fabrication and characterization of a bismuth nanoparticle modified boron doped diamond electrode and its application to the simultaneous determination of cadmium(II) and lead(II). *Electroanal.* 2008;20:1731–1737. doi:[10.1002/elan.200804277](#)
- Nguyen LD, Doan TCD, Huynh TM, Nguyen VNP, Dinh HH, Dang DMT, Dang CM. An electrochemical sensor based on polyvinyl alcohol/chitosan-thermally reduced graphene composite modified glassy carbon electrode for sensitive voltammetric detection of lead. *Sensors Actuators B Chem.* 2021;345:130443. doi:[10.1002/elan.200804277](#)
- Mardegan A, DalBorgo S, Scopece P, Moretto LM, Hočevar SB, Ugo P. Simultaneous adsorptive cathodic stripping voltammetric determination of nickel(ii) and cobalt(ii) at an in situ bismuth-modified gold electrode. *Electroanal.* 2013;25:2471–2479. doi:[10.1002/elan.201300320](#)
- Nigović B, Šimunić B, Hočevar S. Voltammetric measurements of aminosalicylate drugs using bismuth film electrode. *Electrochim Acta.* 2009;54:5678–5683. doi:[10.1016/j.electacta.2009.05.006](#)
- Jovanovski V, Hočevar SB, Ogorevc B. Ex situ prepared antimony film electrode for electrochemical stripping measurement of heavy metal ions. *Electroanal.* 2009;21:2321–2324. doi:[10.1002/elan.200904692](#)
- Zhu WW, Li NB, Luo HQ. Simultaneous determination of chromium(III) and cadmium(II) by differential pulse anodic stripping voltammetry on a stannum film electrode. *Talanta.* 2007;72:1733–1737. doi:[10.1016/j.talanta.2007.04.055](#)
- Economou A, Fielden PR. Mercury film electrodes: Developments, trends and potentialities for electroanalysis. *Analyst.* 2003;2:814–815. doi:[10.1039/b201130c](#)
- Kokkinos C, Economou A. Stripping analysis at bismuth-based electrodes. *Curr Anal Chem.* 2008;4:183–190. doi:[10.2174/157341108784911352](#)
- Serrano N, Díaz-Cruz JM, Ariño C, Esteban M. Antimony-based electrodes for analytical determinations. *TRAC – Trends Anal Chem.* 2016;77:203–213. doi:[10.1016/j.trac.2016.01.011](#)
- Wang J, Lu J, Hočevar SB, Farias PAM, Ogorevc B. Bismuth-coated carbon electrodes for anodic stripping voltammetry. *Anal Chem.* 2000;72:3218–3222. doi:[10.1021/ac000108x](#)
- Economou A. Screen-printed electrodes modified with “green” metals for electrochemical stripping analysis of toxic elements. *Sensors.* 2018;18:1032.
- Bi Z, Chapman CS, Salaün P, Van Den Berg CMG. Determination of lead and cadmium in sea- and freshwater by anodic stripping voltammetry with a vibrating bismuth electrode. *Electroanal.* 2010;22:2897–2907. doi:[10.1002/elan.201000429](#)
- Seifi A, Afkhami A, Madrakian T. Highly sensitive and simultaneous electrochemical determination of lead and cadmium ions by poly(thionine)/MWCNTs-modified glassy carbon electrode in the presence of bismuth ions. *J Appl Electrochem.* 2022;52:1513–1523. doi:[10.1007/s10800-022-01728-4](#)
- Alves GMS, Magalhães JMCS, Soares HMVM. Simultaneous determination of nickel and cobalt using a solid bismuth vibrating electrode by adsorptive cathodic stripping voltammetry. *Electroanal.* 2013;25:1247–1255. doi:[10.1002/elan.201200643](#)
- Hočevar SB, Švancara I, Ogorevc B, Vytřas K. Antimony film electrode for electrochemical stripping analysis. *Anal Chem.* 2007;79:8639–8643. doi:[10.1021/aco70478m](#)
- Pérez-Ràfols C, Serrano N, Díaz-Cruz JM, Ariño C, Esteban M. New approaches to antimony film screen-printed electrodes using carbon-based nanomaterials substrates. *Anal Chim Acta.* 2016;916:17–23. doi:[10.1016/j.aca.2016.03.003](#)
- Sebez B, Ogorevc B, Hočevar SB, Veber M. Functioning of antimony film electrode in acid media under cyclic and anodic stripping voltammetry conditions. *Anal Chim Acta.* 2013;785:43–49. doi:[10.1016/j.aca.2013.04.051](#)
- Barceló C, Serrano N, Ariño C, Díaz-Cruz JM, Esteban M. Ex situ antimony screen-printed carbon electrode for voltammetric determination of Ni(ii)-ions in wastewater. *Electroanalysis.* 2016;28:640–644. doi:[10.1002/elan.201500511](#)
- Tapia MA, Pérez-Ràfols C, Paštika J, Gusmão R, Serrano N, Sofer Z, Díaz-Cruz JM. Antimony nanomaterials modified screen-printed electrodes for the voltammetric determination of metal ions. *Electrochim Acta.* 2022;425. doi:[10.1016/j.electacta.2022.140690](#)
- Czop E, Economou A, Bobrowski A. A study of in situ plated tin-film electrodes for the determination of trace metals by means of square-wave anodic stripping voltammetry. *Electrochim Acta.* 2011;56:2206–2212. doi:[10.1016/j.electacta.2010.12.017](#)
- Švancara I, Prior C, Hočevar SB, Wang J. A decade with bismuth-based electrodes in electroanalysis. *Electroanal.* 2010;22:1405–1420. doi:[10.1002/elan.200970017](#)
- Rojas-Romo C, Aliaga ME, Arancibia V. Determination of molybdenum(VI) via adsorptive stripping voltammetry using an ex-situ bismuth screen-printed carbon electrode. *Microchem J.* 2020;154:104589. doi:[10.1016/j.microc.2019.104589](#)
- Tapia MA, Pérez-Ràfols C, Oliveira FM, Gusmão R, Serrano N, Sofer Z, Díaz-Cruz JM. Antimonene-modified screen-printed carbon nanofibers electrode for enhanced electroanalytical response of metal ions. *Chemosensors.* 2023;11:219. doi:[10.3390/chemosensors11040219](#)
- Ivoilova A, Malakhova N, Mozharovskaia P, Nikiforova A, Tumashov A, Kozitsina A, Ivanova A, Rusinov V. Study of different carbonaceous materials as modifiers of screen-printed carbon electrodes for the triazid as potential antiviral drug. *Electroanal.* 2022;34:1745–1755. doi:[10.1002/elan.202100657](#)
- Christidi S, Chrysostomou A, Economou A, Kokkinos C, Fielden PR, Baldock SJ, Goddard NJ. Disposable injection molded conductive electrodes modified with antimony film for the electrochemical determination of trace Pb(II) and Cd(II). *Sensors (Switzerland).* 2019;19:4809. doi:[10.3390/s19214809](#)

26. Dal Borgo S, Jovanovski V, Hocevar SB. Antimony film electrode for stripping voltammetric measurement of Hg(II) in the presence of Cu(II). *Electrochim Acta*. 2013;88:713–717. doi:[10.1016/j.electacta.2012.10.122](https://doi.org/10.1016/j.electacta.2012.10.122)
27. Sopha H, Jovanovski V, Hocevar SB, Ogorevc B. *In-situ* plated antimony film electrode for adsorptive cathodic stripping voltammetric measurement of trace nickel. *Electrochem Commun*. 2012;20:23–25. doi:[10.1016/j.elecom.2012.03.048](https://doi.org/10.1016/j.elecom.2012.03.048)
28. Sosa V, Barceló C, Serrano N, Ariño C, Díaz-Cruz JM, Esteban M. Antimony film screen-printed carbon electrode for stripping analysis of Cd(II), Pb(II), and Cu(II) in natural samples. *Anal Chim Acta*. 2015;855:34–40. doi:[10.1016/j.aca.2014.12.011](https://doi.org/10.1016/j.aca.2014.12.011)
29. Arancibia V, Nagles E, Rojas C, Gómez M. Ex situ prepared nafion-coated antimony film electrode for adsorptive stripping voltammetry of model metal ions in the presence of pyrogallol red. *Sensors Actuators B Chem*. 2013;182:368–373. doi:[10.1016/j.snb.2013.03.014](https://doi.org/10.1016/j.snb.2013.03.014)
30. Kokkinos C, Economou A, Raptis I, Speliotis T. Novel disposable microfabricated antimony-film electrodes for adsorptive stripping analysis of trace Ni(II). *Electrochem Commun*. 2009;11:250–253. doi:[10.1016/j.elecom.2008.11.022](https://doi.org/10.1016/j.elecom.2008.11.022)
31. Pérez-Ràfols C, Trechera P, Serrano N, Díaz-Cruz JM, Ariño C, Esteban M. Determination of Pd(II) using an antimony film coated on a screen-printed electrode by adsorptive stripping voltammetry. *Talanta*. 2017;167:1–7. doi:[10.1016/j.talanta.2017.01.084](https://doi.org/10.1016/j.talanta.2017.01.084)
32. Nigović B, Hocevar SB. Square-wave voltammetric determination of pantoprazole using exsitu plated antimony-film electrode. *Electrochim Acta*. 2013;109:818–822. doi:[10.1016/j.electacta.2013.07.173](https://doi.org/10.1016/j.electacta.2013.07.173)
33. Betancourth JM, Cuellar M, Ortiz PI, Pfaffen V. Multivariate cathodic square wave stripping voltammetry optimization for nitro group compounds determination using antimony film electrodes. *Microchem J*. 2018;139:139–149. doi:[10.1016/j.microc.2018.02.028](https://doi.org/10.1016/j.microc.2018.02.028)
34. Zhu WW, Li NB, Luo HQ. Simultaneous determination of chromium(III) and cadmium(II) by differential pulse anodic stripping voltammetry on a stannum film electrode. *Talanta*. 2007;72:1733–1737. doi:[10.1016/j.talanta.2007.04.055](https://doi.org/10.1016/j.talanta.2007.04.055)
35. Tian YQ, Li NB, Luo HQ. Simultaneous determination of trace zinc(II) and cadmium(II) by differential pulse anodic stripping voltammetry using a MWCNTs-NaDBS modified stannum film electrode. *Electroanal*. 2009;21:2584–2589. doi:[10.1002/elan.200900249](https://doi.org/10.1002/elan.200900249)
36. Scholz F. *Electroanalytical methods: guide to experiments and applications*, 2nd Edition. Germany: Springer; 2010. 347 p.
37. Ortiz B, Saby C, Champagne GY, Bélanger D. Electrochemical modification of a carbon electrode using aromatic diazonium salts. 2. Electrochemistry of 4-nitrophenyl modified glassy carbon electrodes in aqueous media. *J Electroanal Chem*. 1998;455:75–81. doi:[10.1016/S0022-0728\(98\)00252-69](https://doi.org/10.1016/S0022-0728(98)00252-69)
38. Rooney MB, Coomber DC, Bond AM. Achievement of near-reversible behavior for the $[\text{Fe}(\text{CN})_6]^{3-/4-}$ redox couple using cyclic voltammetry at glassy carbon, gold, and platinum macro-disk electrodes in the absence of added supporting electrolyte. *Anal Chem*. 2000;72:3486–3491. doi:[10.1021/ac991464m](https://doi.org/10.1021/ac991464m)
39. Muna GW, Barrera E, Robinson L, Majeed H, Jones K, Damschroder A, Vila A. Electroanalytical performance of a Bismuth/Antimony composite glassy carbon electrode in detecting lead and cadmium. *Electroanal*. 2023;35:1–12. doi:[10.1002/elan.202300019](https://doi.org/10.1002/elan.202300019)
40. Malakhova N, Kifle AB, Ivoilova A, Leonova N, Kozitsina A. Neutral red as a redox probe for comparative evaluation of electrochemical performance of bismuth modified electrodes. *Anal Lett*. 2024:1–18. doi:[10.1080/00032719.2024.2314744](https://doi.org/10.1080/00032719.2024.2314744)
41. Nigović B, Hocevar SB. Square-wave voltammetric determination of pantoprazole using ex situ plated antimony-film electrode. *Electrochim Acta*. 2013;109:818–822. doi:[10.1016/j.electacta.2013.07.173](https://doi.org/10.1016/j.electacta.2013.07.173)
42. Alves GMS, Rocha LS, Soares HMVM. Multi-element determination of metals and metalloids in waters and wastewaters, at trace concentration level, using electroanalytical stripping methods with environmentally friendly mercury free-electrodes: A review. *Talanta*. 2017;175:53–68. doi:[10.1016/j.talanta.2017.06.077](https://doi.org/10.1016/j.talanta.2017.06.077)
43. Nigović B, Hocevar SB. Antimony film electrode for direct cathodic measurement of sulfasalazine. *Electrochim Acta*. 2011;58:523–527. doi:[10.1016/j.electacta.2011.09.087](https://doi.org/10.1016/j.electacta.2011.09.087)
44. Walz Jr F.G., Terenna B., Rolince D.. Equilibrium studies on neutral red–DNA binding. *Biopolym. Orig. Res. Biomol*. 1975;14:825–837.
45. Halliday CS, Matthews DB. Some electrochemical and photoelectrochemical properties of 3-Amino-7-dimethylamino-2-methylphenazine (Neutral Red) in aqueous solution. *Austral J Chem*. 1983;36:507–516.
46. Pauliukaite R, Ghica ME, Barsan M, Brett CMA. Characterisation of poly(neutral red) modified carbon film electrodes; Application as a redox mediator for biosensors. *J Solid State Electrochem*. 2007;11:899–908. doi:[10.1007/s10008-007-0281-9](https://doi.org/10.1007/s10008-007-0281-9)
47. Jeykumari DRS, Narayanan SS. Covalent modification of multiwalled carbon nanotubes with neutral red for the fabrication of an amperometric hydrogen peroxide sensor. *Nanotechnology*. 2007;18: 125501. doi:[10.1088/0957-4484/18/12/125501](https://doi.org/10.1088/0957-4484/18/12/125501)
48. Kaur B, Srivastava R. Simultaneous determination of epinephrine, paracetamol, and folic acid using transition metal ion-exchanged polyaniline-zeolite organic-inorganic hybrid materials. *Sensors Actuators B Chem*. 2015;211:476–488. doi:[10.1016/j.snb.2015.01.081](https://doi.org/10.1016/j.snb.2015.01.081)
49. Hong J, Kim K. Neutral red and ferroin as reversible and rapid redox materials for redox flow batteries. *ChemSusChem*. 2018;11:1866–1872. doi:[10.1002/cssc.201800303](https://doi.org/10.1002/cssc.201800303)
50. Li Z, Zhou Z, Yun G, Shi K, Lv X, Yang B. High-performance solid-state supercapacitors based on graphene-ZnO hybrid nanocomposites. *Nanoscale Res Lett*. 2013;8:473. doi:[10.1186/1556-276X-8-473](https://doi.org/10.1186/1556-276X-8-473)
51. Ranjan B, Kaur D. Pseudocapacitive storage in molybdenum oxynitride nanostructures reactively sputtered on stainless-steel mesh towards an all-solid-state flexible supercapacitor. *Small*. 2023;2307723:1–17. doi:[10.1002/sml.202307723](https://doi.org/10.1002/sml.202307723)
52. Stoynov ZB, Grafov BM, Savova-Stoynov BS, Elkin VV. *Electrochemical Impedance*. Moscow: Nauka; 1991. 336 p. Russian.
53. Finšgar M, Kovačec L. Copper-bismuth-film in situ electrodes for heavy metal detection. *Microchem J*. 2020;154:104635. doi:[10.1016/j.microc.104635](https://doi.org/10.1016/j.microc.104635)
54. Vladislavić N, Buzuk M, Brinić S, Buljac M, Bralić M. Morphological characterization of ex situ prepared bismuth film electrodes and their application in electroanalytical determination of the biomolecules. *J Solid State Electrochem*. 2016;20(8):2241–2250. doi:[10.1007/s10008-016-3234-3](https://doi.org/10.1007/s10008-016-3234-3)
55. Yates F. *Statistical tables for biological agricultural and medical research*. London: Bookliver and Bookyd; 1938. 90 p.